ELSEVIER

Nuclear Physics A626 (1997) 287c–294c

NUCLEAR PHYSICS A

Probing the nuclear EOS with GeV light-ion beams

V.E. Viola[a], W.-c. Hsi[a], K. Kwiatkowski[a], G. Wang[a], D.S. Bracken[a†], H. Breuer[b], J. Brzychczyk[c], Y.Y. Chu[d], E. Cornell[a], E. Renshaw Foxford[a], F. Gimeno-Nogues[e], D. Ginger[a], S. Gushue[d], M.J. Huang[f], R.G. Korteling[g], R. Legrain[h], W.G. Lynch[f], K.B. Morley[a], E.C. Pollacco[h], E. Ramakrishnan[e], L.P. Remsberg[d], D. Rowland[e], M.B. Tsang[f], C. Volant[h], H. Xi[f], S.J. Yennello[e] and N.R. Yoder[a]

[a]Indiana University, Bloomington, IN 47405
[b]University of Maryland, College Park, MD 20742
[c]Jagiellonian University, Krakow, Poland
[d]Brookhaven National Laboratory, Upton, NY 11973
[e]Texas A & M University, College Station, TX
[f]Michigan State University, East Lansing, MI 48824
[g]Simon Fraser University, Burnaby, B.C., Canada
[h]CEA Saclay, Gif-sur-Yvette 91191, France

The first 4π studies of identified light-charged-particles and IMFs emitted in the p, π^- + ^{197}Au reactions above 5 GeV/c are reported. Multiplicity and angular distributions show little sensitivity to either bombarding energy or projectile type. Excitation energy distributions obtained from data for the 4.8 GeV ^{3}He + ^{197}Au reaction yield values up to $E^* \lesssim 1500$ MeV and $E^*/A_{residue} \lesssim 10$ MeV/nucleon. Analysis of large-angle, IMF-IMF correlations for this same system suggests that multifragmentation is a fast, time-dependent process.

1. INTRODUCTION

Central collisions induced by GeV light-ion beams provide an important means of rapidly heating the nuclear liquid close to the vaporization regime [1-3]. Hard nucleon-nucleon scatterings and the formation of multiple Δ (and higher) resonances initiate the excitation, creating a localized region of "resonance matter" in the core of the struck nucleus. Randomization of the contained nucleons and resonance decay/pion reabsorption processes then create nuclear matter at high temperatures (T ~ 15 MeV) on a short time scale, $\tau \lesssim 40$ fm/c [2,3]. Subsequently, the nucleus expands and cools into the liquid-gas coexistence and spinodal instability regimes of the nuclear phase diagram. This mechanism is in contrast with the collective compression/decompression mechanism believed to be responsible for producing similarly unstable systems in heavy-ion reactions. Understanding the dynamics of these complex processes is vital to determining the properties of the nuclear equation of state (EOS) as a function of temperature, density and isospin.

PII S0375-9474(97)00549-6

While the light-ion EOS studies described in this report were performed with external beams at the Laboratoire National Saturne and the Brookhaven AGS, they represent an important class of experiments that could be performed with stored beams of 2 - 15 GeV light ions; for example, the LISS facility proposed for Indiana University. Stored antiproton beams are of similar interest. One of the striking features of studies thus far is that the debris formed in the most violent collisions--from which we must deduce the parameters of the nuclear EOS--is rich in very low-energy light-charged particles and IMFs (IMF: $3 \le Z \le 20$). Thus, stored beams possess many advantages for the experiments required to study these phenomena, which require high granularity 4π detection systems having a broad dynamic range in energy acceptance. Among these advantages are ultra thin targets, precise spatial resolution of the beam, clean primary beam, and fast-timing capabilities. All of these features are needed to define precise ejectile energy spectra, which are our most sensitive probe of nuclear expansion and directly related to the nuclear compressibility.

The measurements reported here were performed during E228 at LNS and E900 at AGS using the Indiana Silicon Sphere 4π detector array [4]. Many results of the LNS experiments have been published previously in Refs. 5 and 6. In this paper, we first examine recent results from proton- and π^--induced reactions on ^{197}Au nuclei. Then the salient conclusions of previous studies with ^{3}He beams on ^{197}Au are reviewed, followed by two new analyses of these data relevant to the questions of excitation energy distributions and the time evolution of these reactions. In the summary, we suggest a scenario for describing these multifragmentation phenomena.

2. THE π^-, p + ^{197}Au REACTIONS

Exclusive excitation functions for charged-particle emission in the 5.0 - 9.2 GeV/c π^- + ^{197}Au and 6.0 - 14.6 GeV/c ^{197}Au reactions were measured with the ISiS array. Secondary beams from the AGS production target were used in these studies; here we associate protons with the positive beam and π^- with the negative beam. The ISiS array was complemented by

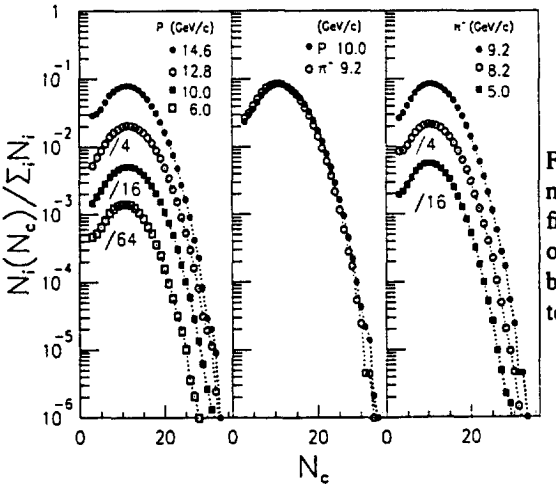

Figure 1. Probability distributions for measured charged-particle multiplicities from ^{197}Au target for events with at least one IMF. Left: proton beams; right: π^- beams, and center: p and π^- at 9.1 GeV total energy.

an upstream beam-counter/defining scintillator and a dual inner/outer scintillator array for halo rejection and beam alignment. The multiplicity trigger required signals in three or more of the 162 silicon detectors in the array. In order to provide information on the multiplicity of fast cascade particles, all CsI signals with energy greater than 8 MeV (but ΔE too low to trigger the corresponding silicon CFD) were also recorded.

In Fig. 1, the measured charged-particle distributions are shown for events in which at least one IMF is observed. The left-hand frame compares the probability distributions for total charged multiplicities obtained with proton beams (6.2, 10.0, 12.8, and 14.6 GeV/c) and the right-hand frame provides the same information for π^- beams (5.0, 8.2 and 9.2 GeV/c). The center frame compares p and π^- projectiles at the same total kinetic energy of 9.1 GeV. Similarly, the measured IMF probability distributions are shown in Fig. 2; i.e. proton results on the left, pion results on the right and the 9.1 GeV kinetic energy π^-/p comparison in the center. IMF-correlated charged particle multiplicities up to N_c ~ 30 are seen in each case, with a most probable value of about N_c ~ 10. IMF multiplicities up to N_{IMF} = 9 - 10 are measured for each system, with an average measured value of $\langle N_{IMF} \rangle$ ~ 1.6 - 1.7.

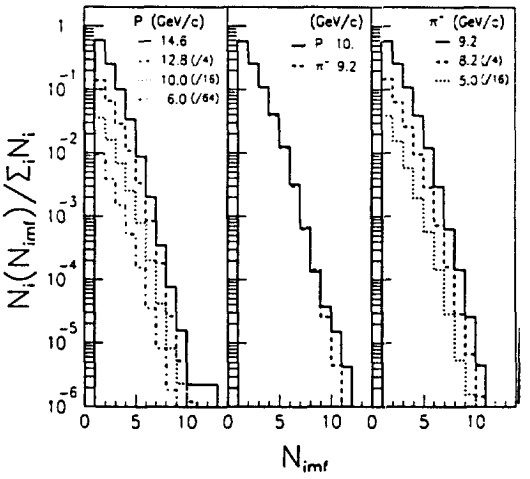

Figure 2. Probability distributions for measured IMF multiplicities from ^{197}Au target for events with at least one IMF. Left: proton beams; right: π^- beams, and center: p and π^- at 9.1 GeV total energy.

Two features stand out in the comparisons of Figs. 1 and 2. First, there is little sensitivity to bombarding energy with either projectile. This result is consistent with the observation of limiting fragmentation in these reactions [7] and reflects a saturation in deposition energy in the vicinity of beam momenta above about 6 GeV/c, similar to that previously reported for ^{3}He projectiles [5]. The second observation is that for identical total kinetic energy, the p and π^- distributions for both charged particles and IMFs are nearly identical. This similarity suggests that the proton and negative pion are equally effective in depositing energy in the target nucleus. Both the bombarding-energy and hadron-type independence are in agreement with the intranuclear cascade code of Toneev [8].

The average measured IMF multiplicity $\langle N_{IMF} \rangle$ for events in which one or more IMFs are emitted is shown in Fig. 3 as a function of beam energy. These values do not include geometry or energy-threshold corrections, which are nearly the same in all cases. Also plotted are values of $\langle N_{IMF} \rangle$ for the p + ^{197}Au reaction at 200 MeV [9], and ^{3}He + ^{197}Au reaction at 1.8 GeV and 4.8 GeV [5,6]. Our results are significantly lower (~ 60%) than reported in Ref. 10, in which IMF Z determination was not performed. Also shown in Fig. 3 is the average IMF multiplicity when at least half of the target charge is detected in the ISiS array. This illustrates that the selection of more violent collisions significantly enhances the average number of IMFs per event. In this regard, these IMF multiplicity results are comparable to the 4.8 GeV ^{3}He + ^{197}Au [5,6] and 6 GeV ^{86}Kr + ^{197}Au reactions [11].

Angular distributions for these reactions have also been investigated for $3 \leq Z < 25$ fragments. The inclusive differential cross sections are gently forward peaked, with forward-to-backward ratios ~ 2:1. However, with increasing IMF charge or multiplicity, the angular distributions become progressively more isotropic, indicating a low-velocity source that is in "kinetic equilibrium"; i.e. the momenta of the residue nucleons have been randomized prior to fragment emission.

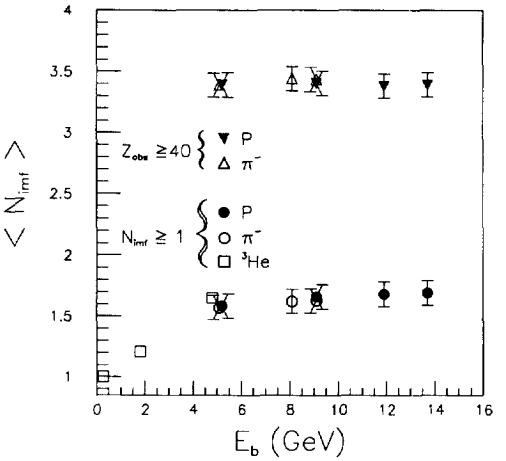

Figure 3. Average observed IMF multiplicity as a function of bombarding energy for the ^{197}Au target; closed symbols are for p data; open for π^-, and squares for ^{3}He. Circles are for events in which one or more IMFs is emitted; triangles are for events in which over 50% of the target charge is observed.

3. EXCITATION ENERGY DEPOSITION

In the remainder of this report, we examine recent results from the 4.8 GeV ^{3}He + ^{197}Au reaction. Previous analyses of the 1.8 - 4.8 GeV ^{3}He + Ag, Au reactions [5,6] have demonstrated the following features:

(1) Multiplicity distributions for the ^{3}He + ^{nat}Ag case suggest a saturation in deposition energy above a bombarding energy of about 4 GeV;

(2) Rapidity distributions indicate an average source in "kinetic equilibrium" with velocities $v \approx 0.01$ c;

(3) Moving-source fits to the spectra indicate expansion to a value of $\rho/\rho_0 \leq 1/3$ at breakup [12];
(4) The cross section for multifragmentation events ($M_{IMF} \geq 3$) at 4.8 GeV is about 40 mb for Ag and 200 mb for ^{197}Au, and
(5) Small-angle correlations yield breakup time scales of < 100 fm/c for high multiplicity events [13].

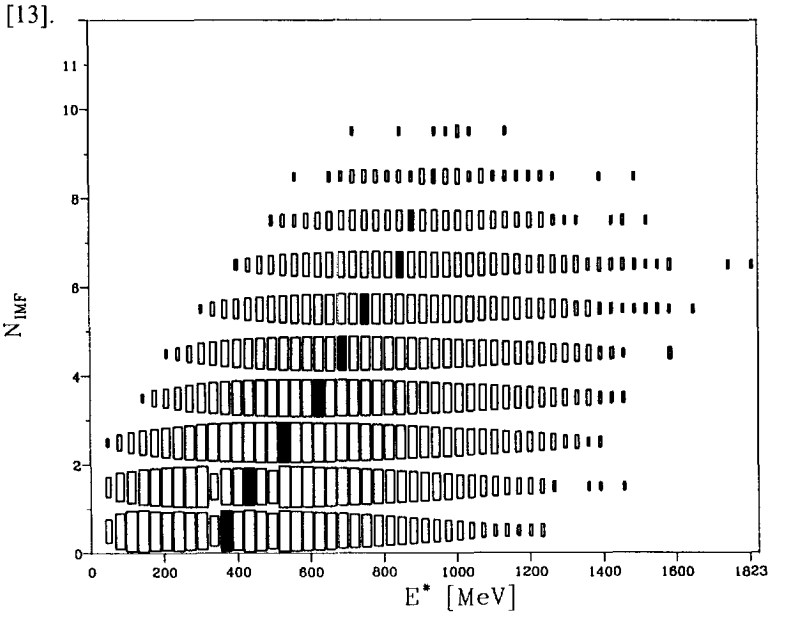

Figure 4. Excitation energy for the 4.8 GeV ^{3}He + ^{197}Au system as a function of observed IMF multiplicity.

A question of central importance in interpreting multifragmentation data in terms of the nuclear EOS is the excitation energy of the fragmenting system. For the 4.8 GeV ^{3}He + ^{197}Au system, excitation energies have been reconstructed from the measured data, where

$$E^* = \sum_{M_{CP}}^{CP} E_K(i) + \sum_{n}^{M_n} E_n(i) + Q \qquad (1)$$

Here $E_K(I)$ represents the measured kinetic energy of each thermal charged particle, corrected for geometry; fast cascade preequilibrium events are eliminated from this sum according to procedures outlined in Ref. 5. The neutron multiplicity distributions are based on experimental results for similar systems [14] and the kinetic energy component is scaled according to Coulomb-corrected light-charged-particle spectra. Q values are then calculated from the binding energies of each ejectile in an event, with the Z and A of the source being determined from

$$(A,Z)_{source} = (A,Z)_{target} - \sum (A,Z)_{fast} \quad (2)$$

where $(A,Z)_{fast}$ represents the measured fast-cascade/preequilibrium component in an event, corrected for geometry and neutron multiplicity assuming $M_n(fast) = (N/Z)_{target} M_{CP}(fast)$. In Fig. 4, the excitation energy distribution is plotted for each of the observed IMF multiplicities. Values below 150 MeV are not meaningful due to the multiplicity trigger of two in this case and the strong dominance of neutron emission for low deposition energies. The preliminary results show that total E* values up to 1500 MeV and $E^*/A \lesssim 10$ MeV/residue nucleon are reached in these collisions, comparable to the total nuclear binding energy. The centroids are also indicated in Fig. 4 and demonstrate a systematic increase in the average excitation energy as a function of increasing IMF multiplicity, consistent with theoretical predictions [15-17].

4. TIME DEPENDENCE

Because of the strong influence of the Coulomb interaction on nuclei undergoing multifragment disintegration, relative velocities (v_{rel}) of fragment pairs emitted at large angles with respect to one another provide a useful probe of the time evolution of the system and the source dimensions at freezeout [18-20]. In this analysis, IMF pairs with $3 \lesssim Z \lesssim 15$ were sampled for polar angles greater than 30° and separation angles $\psi_{rel}(1,2) = 180° \pm 40°$. The IMF velocity acceptance was $2.3 \lesssim v_{rel} \lesssim 8.8$ cm/ns, with the upper limit chosen to minimize nonequilibrium contributions to the spectra [5]. Relative velocities were calculated from the fragment energies, using average masses, as measured in Refs. 19 and 20. Data points represent the average of these two measurements and error bars indicate the upper and lower limits.

In Fig. 5 (left frame) the centroids of the relative velocity distributions are shown for various IMF multiplicity bins. The centroids evolve monotonically toward lower v_{rel} values with increasing fragment charge; however, there appears to be little sensitivity to collision violence in these results. In order to establish a baseline for comparing the sensitivity of the v_{rel} data to the Coulomb field of the emitting source, the data are compared with values based on fission kinetic-energy-release systematics [21]. The Z and A of the fissioning source are estimated from well-tested intranuclear cascade calculations [22], which are in general agreement with the reconstructed distributions discussed in Section 3. The shaded region in the left-hand frame of Fig. 5 represents the range of these predictions. Comparison of the data with this empirical Coulomb-repulsion model indicates that for the heaviest IMFs, there is good agreement for all IMF multiplicities. The corresponding radius parameter for axial charge separation ($r_0 = 1.80$ fm) in fission is also consistent with emission from a radially expanding source with $\rho/\rho_0 \sim 0.3 - 0.5$. As the charge of the IMF pair decreases, however, the centroids of the v_{rel} distributions diverge significantly above the fission Coulomb systematics. This suggests that on average, lighter IMFs have their origin in more dense/hotter/higher charge sources, regardless of IMF multiplicity. These observations favor a time-dependent picture of light-ion-induced multifragmentation in which light fragments ($Z \lesssim 8$) are emitted from a hot, expanding source, followed by breakup of a dilute residue in which all IMF charges are emitted.

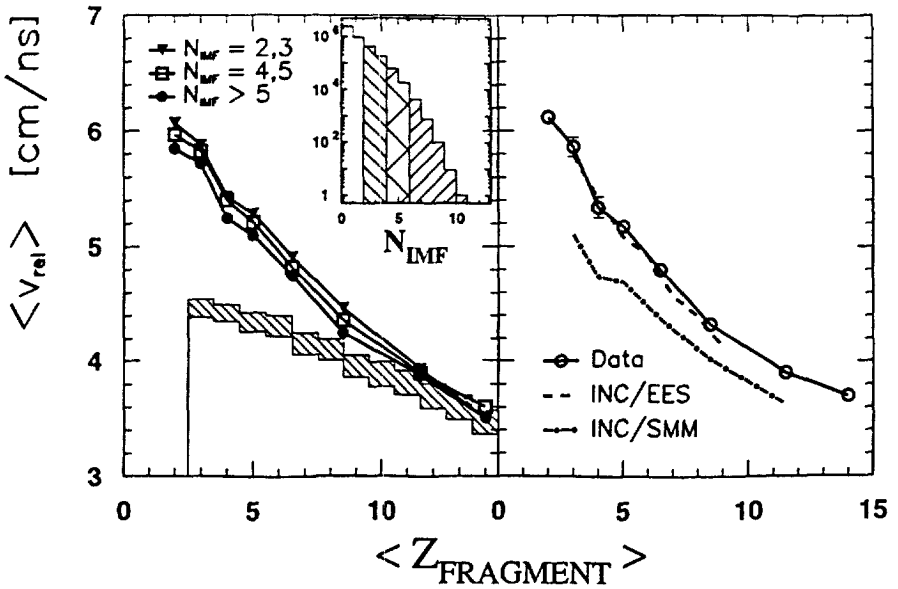

Figure 5. Centroids of relative IMF-IMF velocity distributions as a function of IMF charge. Left frame gives data as a function of IMF multiplicity; shaded area is range of values predicted by fission Coulomb energy systematics. Right frame gives data for all multiplicities compared with hybrid model predictions of INC/EES model (dashed line) and INC/SMM model (dot-dashed line).

In the right-hand frame of Fig. 5, the experimental relative-velocity centroids for IMF pairs of all multiplicities are compared with predictions based on two hybrid models. Identical INC calculations provided the distribution of residue mass, charge and excitation energy produced in the fast-cascade phase of the reaction. These then served as input for two models which differ significantly in their assumptions about the time evolution of the IMF emission process. These were the time-dependent expanding emitting source model [15] and the simultaneous statistical multifragmentation SMM model [23]. The default conditions of both models were employed, most importantly, a value of K = 144 MeV for the effective compressibility parameter in the EES model and a breakup density of $\rho/\rho_0 = 1/3$ in the SMM case. These default conditions have proved successful in describing heavy-ion multi-fragmentation. Experimental thresholds were imposed on the calculations.

The comparison of the INC/EES calculations with the data shows good agreement for all values of Z. The INC/SMM model accounts for the heavier fragments relatively well and can be improved by increasing the critical breakup density from the default value to $\rho/\rho_0 \sim ½$. However, this does not alter the curvature of the predictions and thus underestimates the Z = 3 - 6 data significantly. The overall agreement of the INC/EES calculation relative to the INC/SMM model appears to be due to the pre-breakup IMF emission stage in the former model--which bridges the time interval between the initial fast cascade and multifragmentation-breakup stages of the reaction. This time-dependent scenario is thus consistent with that deduced from comparison with empirical Coulomb systematics.

5. SUMMARY

Recent measurements at AGS have demonstrated that 5 - 15 GeV/c hadron-induced reactions on ^{197}Au produce multifragmentation observables similar in most respects to ^{3}He and heavy-ion projectiles [5,6,11]. In this energy range, there is little sensitivity to either bombarding energy or hadron type, consistent with both INC calculations [8] and IMF excitation function data [7,20]. Excitation-energy distributions have been derived for the 4.8 GeV ^{3}He + ^{197}Au system. These show maximum values of E* ~ 1500 MeV and E*/A ~ 10 MeV/residue nucleon and a monotonic increase in E*/A with increasing IMF multiplicity. Analysis of large-angle IMF-IMF correlations yields a time-dependent picture of light-ion-induced multifragmentation in which the fast cascade produces a hot, expanding residue. Light fragments ($Z \lesssim 8$) are emitted sequentially during the expansion, followed by cooling and multifragmentation of the residues at a breakup density $\rho/\rho_0 < \frac{1}{2}$. Comparisons with INC/EES and INC/SMM model predictions are consistent with the data for heavier fragments.

The authors acknowledge the primary support of the U.S. DOE for these studies. Additional support was provided by the U.S. National Science Foundation, NSERC of Canada and CEA Saclay.

REFERENCES

1. H. Müller and B.D. Serot, Phys. Rev. C., 52 (1995) 2072.
2. J. Cugnon et al., Nucl. Phys. A, 379, (1982) 533; 462 (1987) 751.
3. G. Wang et al., Phys. Rev. C, 53 (1996) 1811.
4. K. Kwiatkowski et al., Nucl. Instr. Meth. A, 360 (1995) 571.
5. K.B. Morley et al., Phys. Rev. C, 54 (1996) 737.
6. E. Renshaw Foxford et al., Phys. Rev. C, 54 (1996) 749.
7. G. Rudstam, Z. Naturforsch. Teil A, 21a (1966) 1027.
8. V. Toneev et al., Nucl. Phys. A, 519 (1990) 463c.
9. D.S. Ginger et al., Indiana Nuclear Chemistry Report INC-40007-112 (1996) 11.
10. V.A. Karnaukhov et al., JINR Dubna preprint E1-96-50.
11. T. Hamilton, Ph.D. thesis, Indiana University (1996).
12. D.S. Bracken, Ph.D. thesis, Indiana University (1996).
13. G. Wang et al., Indiana Nuclear Chemistry Report INC-40007-112 (1996) 21.
14. F. Goldenbaum et al., Phys. Rev. Lett., 77 (1996) 1230; L. Pienkowski et al., Phys. Lett. B, 336 (1994) 147.
15. W.A. Friedman, Phys. Rev. C, 42 (1990) 667.
16. J.P. Bondorf et al., Nucl. Phys. A, 443 (1985) 321; 436 (1985) 265.
17. D.H.E. Gross, Rep. Prog. Phys., 53 (1990) 605; Phys. Letter B, 318 (1993) 405.
18. G. Wang et al., submitted to Phys. Letter
19. R.E.L. Green et al., Phys. Rev. C, 29 (1984) 1806.
20. N.T. Porile et al., Phys. Rev. C, 39 (1989) 1914.
21. V.E. Viola et al., Phys. Rev. C, 31 (1985) 1550.
22. Y. Yariv and Z. Fraenkel, Phys. Rev. C, 20 (1979) 2227; 24 (1991) 488.
23. A. Botvina et al., Nucl. Phys. A, 507 (1990) 649.